Journal of Materials Chemistry B

Accepted Manuscript

ROYAL SOCIETY OF CHEMISTRY

www.rsc.org/materialsB

Cite this: DOI: 10.1039/c0xx00000x

www.rsc.org/xxxxxx

ARTICLE TYPE

Real-time imaging of intracellular drug release from mesoporous silica nanoparticles based on fluorescence resonance energy transfer

Jun Wang, Peng Pei Gao, Xiao Xi Yang, Ting Ting Wang, Jian Wang* and Cheng Zhi Huang*

Received (in XXX, XXX) Xth XXXXXXXXX 20XX, Accepted Xth XXXXXXXXX 20XX

DOI: 10.1039/b000000x

In this study, a targeted cancer therapy, imaging system is designed based on doxorubicin (DOX)-loaded green fluorescence mesoporous silica nanoparticles (FMSN) conjugated with folic acid (FA) by linking α-amine-ω-propionic acid hexaethylene glycol (NH_2-PEG-COOH). In situ formation method is adopted to prepare luminescent MSNs, which then act as the donor of fluorescence resonance energy transfer (FRET) since their emission at 500 nm overlapped with the absorption of acceptor DOX at 485nm. NH_2-PEG-COOH is conjugated to the outer surface of FMSN at one end and modified by folate acid at the other, so that the formed mesoporous silica composite has the merits of fluorescent imaging, mesoporous nanostructure for drug loading, receptor-mediated targeting and real-time monitoring intracellular drug release. It was found that the FA-grafted and PEGlated nanocomposite have excellent biocompatibility toward Hep2 cells, and the cytotoxicity of the loaded-DOX nanoparticles containing the folate targeting units in folate-receptor-rich Hep2 cancer cells is higher than that without folate targeting units under the same conditions. When the resultant nanoparticles enter into the cells, the green fluorescence of FMSN gradually recover along with the release of DOX, so as to achieve the purpose of real-time monitoring of intracellular drug release.

1. Introduction

In the field of human health, one key challenge is how to deliver an effective amount of drug to the targeted sites using non-toxic drug carriers and reduce the toxicity toward other tissues. However, due to poor pharmacokinetic profiles and broad mechanisms of action, only a small amount of the drug is delivered to the disease site.[1] Therefore, to ensure an efficient therapy, a drug carrier should satisfy several prerequisites[2, 3] including good biocompatibility, high drug payloads, avoidance of the burst release, easily monitory such as by visual or imaging techniques, and cell or tissue targeting. In the past decades, several smart bio/nano materials, such as polymers,[4, 5] liposomes,[6, 7] nanoemulsions,[8, 9] dendrimer,[10, 11] hydrogels,[12, 13] gold nanoparticles[14-17] or quantum dots [18-20] (QDs) have been widely investigated for drug delivery. The real case, however, is that it hardly satisfies the above-mentioned prerequisites. Recently, mesoporous silica nanoparticles (MSN) have attracted much attention in the field of nanomedicine. The large surface and pore volume of MSN are suitable for high drug loading or imaging agents. Their highly ordered mesoporous structure avoids the "burst effect". Furthermore, it may offer the possibility to target drug delivery and control release owing to the easy modification of the surface. In addition, the superior biocompatibility of MSN for pharmacological applications has been confirmed.[21, 22] Currently, MSN have been acted as drug carrier to delivery different therapeutic agents for simultaneous imaging and therapeutic applications.[23-27]

Fluorescence resonance energy transfer (FRET) is a non-radiation process in which the energy is transferred from an excited state donor molecule to a ground state acceptor through dipole-dipole interaction.[28-30] The emission of the donor and absorbance of the acceptor must be at the extent of spectral overlap. Being an efficient fluorescence technique, FRET has been widely used in the fields of biochemical sensing and imaging.[31-35] Consequently, the FRET phenomenon can be potentially used to the development of therapeutic approaches for cancer treatment. Recently, Yeung et al.[36] used luciferase chemiluminescence imaging to investigate ATP release from MCM-41-type mesoporous nanosphere. Lee et al.[37] developed a versatile FRET based on MSNs for real-time monitoring of drug release, which is successful with the further two points that should be considered. One is that the mesoporous silica composites whether to be capable of targeted drug delivery, and that other is whether to really achieve real-time monitoring of the whole process of drug release through the FRET. The reason is that the disulfide bond is cleaved by GSH, which triggers the drug release and eliminates FRET. In fact, a smart multifunctional drug carrier should be capable of sensing the drug release in a simple and easily detectable manner.

Based on the aforementioned consideration, we develop a FRET based MSN drug delivery system. The procedure for the synthesis of DOX-FMSN-PEG-FA is shown in Scheme 1. MSNs were initially prepared by the procedure described in the literature.[38, 39] After the removal of the surfactant, the 8-hydroxyquinoline (8-Hq) was embedded into the channels of MSNs containing-zinc ions to form the metalloquinolates by in situ formation method. The formed luminescent MSNs serve as energy donor and drug delivery device. The surface of FMSN was then functionlized with amino groups by refluxing with 3-aminopropyl trimethoxysilane (APTMS), which were further reacted with the carboxyl groups of amino-PEG-Carboxyl (NH_2-PEG-COOH). The anticancer drug doxorubicin as energy acceptor were loaded into the mesopores. Finally, Folic acid (FA) was conjugated to the other end of NH_2-PEG-COOH through the amide reaction for targeted drug delivery. The formed multifunctional nanoparticles could be capable of targeted drug-delivery and sensing the intracellular release of drug. When the nanoparticles enter into the cells, the green fluorescence of FMSN gradually recover along with the release of DOX, so as to achieve the purpose of real-time monitoring of intracellular drug release based on the mechanism of FRET.

2. Experimental section

2.1 Material

Tetraethylorthosilicate (TEOS, 99%), 3-aminopropyl trimethoxysilane (APTMS), and 3-Mercaptopropyltrimethoxysilane (3-MPTS, 95%) were purchased from Sigma-Aldrich. Doxorubicin hydrochloride (DOX·HCl, 98%) was obtained from Dalian Meloney Biotechnology Co., Ltd (Dalian, China). Hexadecyltrimethylammonium chloride (CTACl) was acquired from J&K Technology Co., Ltd. 8-Hydroxyquinoline (8-Hq) and dicyclohexylcarbodiimide hydrochloride (EDC·HCl) were purchased from Aladdin (Shanghai, China). Triethanolamine (TEA) and zinc acetate dehydrate were obtained from Taixin Chemical Co., Ltd (Chongqing, China). Folic acid (FA) was acquired from Beijing Dingguo Changsheng Biotechnology Co., Ltd. α-amine-ω-propionic acid hexaethylene glycol (NH_2-PEG-COOH) was purchased from Jiaxing Bomei Biotechnology Co., Ltd (Zhejiang, China). *N*-hydroxysuccinimide (NHS) was obtained from Acros Organics (New Jersey, America). All other reagents were of analytical grade. Millipore water with 18.2 MΩ was used in the experiment.

2.2 Synthesis of mesoporous silica (MSN-SH)

Colloidal mesoporous silica (CMS) was prepared according to the procedure described in the literature with slight modification.[38, 39] The typical synthetic process is as follows: 14.3 g (96 mmol) of TEA and 2.23 mL (10 mmol) of TEOS plus the corresponding quantity of 1 mmol of 3-MPTS were combined. The two-phase solution was heated in an oil bath at 90 °C for 20 min without stirring. After the mixture was taken out of the oil bath, 26.7 g of aqueous solution (2.5% wt) of CTACl which had been heated to 60 °C was added. The final mixture was stirred (600 rpm) for 3 h at 23 °C. 50 mL of ethanol were added to the translucent, colloidal aqueous suspension, and the resulting precipitate was separated by centrifugation. The final product was dried at room temperature under vacuum.

Template extraction was performed with 15 mL conc. HCl in 120 mL EtOH solution. Usually, the sample was treated two or three times with 120 mL of the extraction solutions by stirring at 60 °C for 12 h. The solid was centrifuged and washed with deionized water for several times. The solid was dried at room temperature under vacuum.

2.3 Synthesis of green fluorescence MSNs (FMSN)

The synthetic progress of mesoporous silica containing zinc 8-hydroxyquinolinate (Znq) were synthesized according to the literature.[40] MSN-SH (0.55 g) were dispersed in aqueous solution of zinc acetate dehydrate (49.7 mL, 0.05 mol/L) and stirred at room temperature for 12 h. The resulting products of Zn^{2+}-containing MSN (MSN-SH-Zn) were collected by centrifugation and washed several times with ethanol. The product was dried at room temperature under vacuum.

The above obtained MSN-SH-Zn (0.49 g) were dispersed in deionized water, then ethanol solution of 8-Hq (0.33 mmol) was added and stirred for 48 h at room temperature. The products were collected by repeated centrifugation and washed several times with ethanol, and then dried at room temperature under vacuum.

2.4 Ammonization of Fluorescent MSN (FMSN-NH_2)

FMSN-NH_2 was prepared according to the literature.[41] 0.45 g of FMSN was refluxed with 80 mL of anhydrous toluene containing 0.75 mL of APTMS for 24 h. The products were collected by centrifugation, washed extensively with deionized water and methanol. The resulting products were dried at room temperature under vacuum.

2.5 Synthesis of FMSN-PEG-NH_2

NH_2-PEG-COOH (100 mg) was activated by EDC·HCl (68 mg) and NHS (38 mg) dissolved in dimethyl sulfoxide (DMSO) (8 mL) solution with stirring for 24 h at 25 °C. Subsequently, the FMSN-NH_2 nanoparticles (100 mg) were added to the activated NH_2-PEG-COOH solution and allowed to react with stirring under anhydrous conditions at 25 °C for 24 h. After the reaction, the mixture was centrifuged and washed with deionized water and ethanol several times to obtain FMSN-PEG-NH_2. The resulting products were dried at room temperature under vacuum.

2.6 Loading of doxorubicin to FMSN -PEG-NH_2

Doxorubicin hydrochloride (7.3 mg) was stirred with FMSN-PEG-NH_2 (80 mg) dispersed in deionized water solution (8 mL) in dark at room temperature for 24 h. The products were collected by repeated centrifugation with deionized water until the supernatant became colorless. The loading efficiency (LE%) of DOX on FMSN-PEG-NH_2 was calculated using the following formula: LE% = $(M_{DOX1}-M_{DOX2})/M_{DOX1}$, where M_{DOX1} is the original DOX content and M_{DOX2} is the unloaded DOX content. The loading content (LC) = (weight of loaded drug / weight of drug carrier).

2.7 Synthesis of DOX-FMSN-PEG-FA

FA (5 mg) was activated by EDC·HCl (30 mg) and NHS (10 mg) dissolved in DMSO (12 mL) solution with stirring for 24 h at 25 °C. Subsequently, the DOX-FMSN-PEG-NH_2 nanoparticles (20 mg) were added to the activated FA solution and allowed to react with stirring for 24 h at 25 °C. After the reaction, the mixture was centrifuged and washed with deionized water and ethanol several times to obtain DOX-FMSN-PEG-FA. The resulting products were dried at room temperature under vacuum.

2.8 In vitro drug release

PBS solutions with pH of 5.0 and 7.4 were first prepared. DOX-FMSN-PEG-FA was dispersed in 2 mL buffer. The dispersion was then transferred into a dialysis bag (molecular weight cut off =14 000 kDa), and the bag was subsequently placed in a 100 mL buffer solution at 37 °C and shaken at 150 rpm. At timed intervals, 5 mL of solution was withdrawn from the solution. The released DOX was analyzed by UV-vis. The volume of the release medium kept constant by adding 5 mL fresh medium after each sampling.

2.9 In vitro cytotoxicity assay

Hep2 cells were seeded into a 96-well plate at a density of 1×10^5 cells per well and cultured at 310 K and 5% CO_2 for 24 h. Then, MSN-SH_1, FMSN-PEG-NH_2, DOX-FMSN-PEG-NH_2, DOX-FMSN-PEG-FA were added to the medium, and the cells were incubated in 5% CO_2 at 310 K for 24 h. Cell viability was determined by MTT assay.

2.10 Cell uptake

Hep2 cells were seeded into 8 mm square glass coverslips placed in 24-well plates and cultured 24 h. The cells were treated with DOX-FMSN-PEG-FA for 12, 24, 36, 48, 72 h (DOX concentration = 2 μg/mL). Then, the cells were washed and fixed with 4% formaldehyde for 30 min. Fluorescence images were observed by confocal laser scanning microscopy (CLSM).

2.11 Characterization

High resolution-transmission electron microscopy (HR-TEM) was conducted on JEM-2100 operated at 200 kV. Zeta potentials were measured on a zeta potential analyzer (Zetasizer Nano ZS90, Malvern). The concentration of DOX solution was measured with a Hitachi UV-3010 spectrometer. The fluorescence spectra of the FMSN derivates were measured with a Hitachi F2500. The surface area, pore size, and pore volume were determined by N_2 adsorption–desorption isotherms obtained at 77 K on a Quantachrome Autosorb-1 (USA). The sample was outgassed at 10^{-3} Torr and 60 °C for approximately 6 h prior to the adsorption experiment. An Olympus IX81LCS-DSU disk scanning confocal microscope (Olympus, Japan) was used for cell imaging. Fourier Transform Infrared (FT-IR) spectra were recorded on a SHIMADZU IRprestige-21 spectrometer.

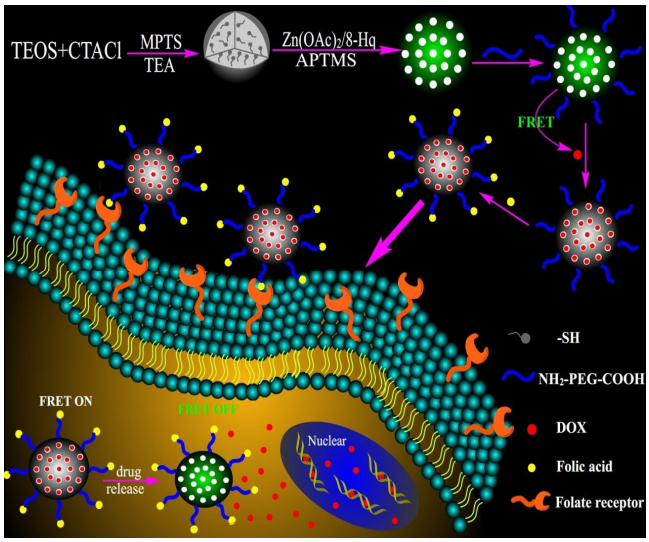

Scheme 1. A diagram showing the synthesis of DOX-FMSN-PEG-FA and sensing of the drug release process by FRET in cancer cell.

3. Results and Discussion

3.1 Preparation and characterization of DOX-FMSN-PEG-FA

Transmission electron microscopy (TEM) images of the MSN-SH nanoparticles are shown in Figure 1A. The higher magnification image revealed that the diameter of MSN-SH nanoparticles was about 60 nm (Figure 1B). When the 8-Hq embedded into the nanoparticles, the nanoparticle shape did not change significantly and the pore structure of nanoparticles still could be seen, indicating that the 8-Hq did not fill the channel of MSN-SH completely and the formed composite still could load drug (Figure 1C and D). In addition, the pore of nanoparticles could not be clearly observed after the conjunction of NH_2-PEG-COOH, due to the masking of the polymers (Figure 1E and F).

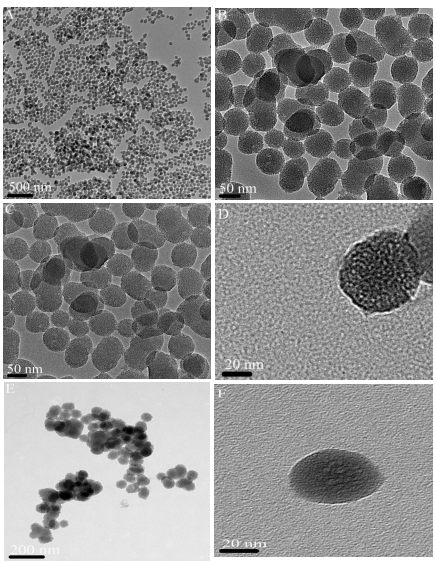

Figure 1. TEM images of the as-prepared MSN-SH (A), FMSN (C), FMSN-PEG-FA (E). Fig. B, D, F is a higher magnification TEM image of MSN-SH, FMSN, FMSN-PEG-FA, respectively.

FT-IR spectra were employed to study each the modification and conjugation process on the nanoparticles (Figure 2A). For pure MSN-SH, the characteristic band of 1085 cm^{-1}, which was attributed to asymmetric stretching vibration of Si-O-Si. Compared to MSN-SH, FMSN displayed additional absorption band of 1578 cm^{-1}, which was attributed to the C–C stretching vibration associated with the quinoline group of ligands Hq. The absorption bands at 1328 and 1393 cm^{-1} involved to the C–C/C–N stretching and C–H bending of the quinoline fragments of Znq [42]. This suggested that the 8-Hq successfully embedded into the channel of the MSN-SH nanoparticles to form metal complex. After ammonization of FMSN, the new emerging absorption band at around 1556 cm^{-1} was assigned to the stretching vibration of $–NH_2$ bending. When NH_2-PEG-COOH was linked to FMSN-NH_2, the feature peaks at 1473 cm^{-1} could be assigned to the stretching vibration of C-C in the NH_2-PEG-COOH chains [43] (Figure 2B).

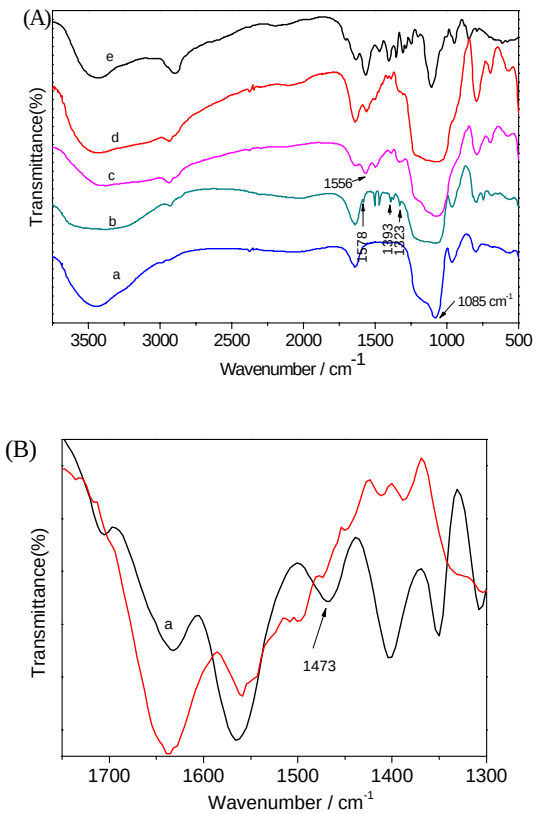

Figure 2. (A) FT-IR spectra of (a) MSN-SH, (b) FMSN, (c) FMSN-NH_2, (d) FMSN-PEG-NH_2 , (e) NH_2-PEG-COOH. (B) Expanded FT-IR spectra of (a) NH_2-PEG-COOH, (b)FMSN-PEG-NH_2.

Consistently, the zeta potential of the resultant nanoparticles are monitored after each modification step (Figure 3). Owing to the existence of Si-OH on the exterior surface of MSN-SH, an approximately -21.7 mV correspond to as prepared MSN-SH. Due to the embedded 8-Hq do not change Si-OH the surface of MSN-SH-Zn, the zeta potential was still -16.3 mV. However, the zeta potential of the FMSN increased from -16.3 mV to +38.9 mV indicating that amino groups anchor on the surface of the nanoparticles. After conjugation of NH_2-PEG-COOH, the obtained nanoparticles still exhibited a zeta potential of +36.7 mV due to the existence of $–NH_2$ on the exterior surface of FMSN-PEG-NH_2 . The FT-IR spectra and zeta potential experiments confirm the successful functionalization MSN-SH nanoparticles. Figure 4 gives the nitrogen adsorption-desorption isotherms and the pore size distribution diagram of the MSN-SH and FMSN. Both samples show the type-Ⅳ isotherms. The embedded 8-Hq into the channel of MSN-SH make the BET surface area, total pore volume, and pore size slightly samller than MSN-SH, which was summarized in Table 1. The test results also confirmed that the pore of MSN-SH was not doped with 8-Hq completely.

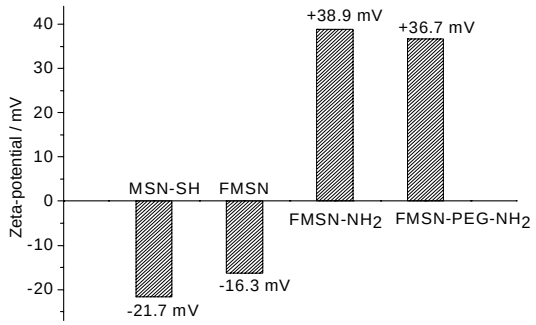

Figure 3. Zeta potential measured at each step of the modification process.

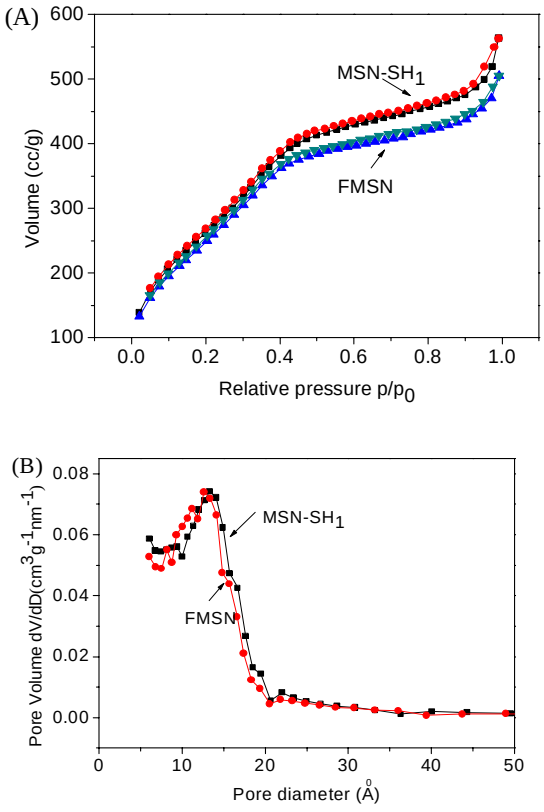

Figure 4. Nitrogen adsorption-desorption isotherms (A) and pore size distributions (B) for the as-synthesized MSN-SH and FMSN.

Figure 5A shows UV-vis absorption spectra of FA, DOX-FMSN-PEG-FA nanoparticles. It can be observed that the main characteristic absorption peak of FA at 280 nm is found in the spectrum of DOX-FMSN-PEG-FA nanoparticles, which suggests that FA has been successfully grafted to the surface of the nanoparticles.

Table 1 Physico-chemical parameters of the MSN-SH and FMSN.

Sample	S_{BET} (m^2/g)	V_{pore} (cm^3/g)	D_{pore} (Å)
MSN-SH	1019	0.87	27
FMSN	968.4	0.78	24

In order to investigate whether each modification change the fluorescence spectrum of the nanoparticles, we measured the fluorescence spectra of FMSN, FMSN-NH_2 and FMSN-PEG-NH_2 nanoparticles. As shown in Figure 5B, it can conclude that each step of the modification does not change the maximum fluorescence emission peak of the nanoparticles.

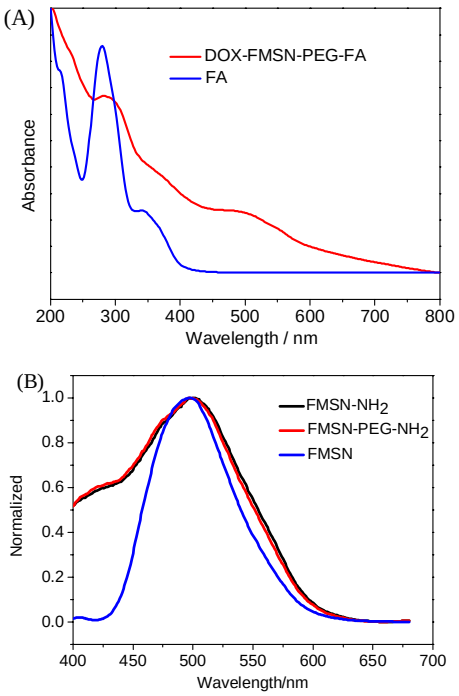

Figure 5. (A) UV/vis spectra of FA, DOX-FMSN-PEG-FA nanoparticles. (B) The fluorescence spectrum of the FMSN, FMSN-NH_2, FMSN-PEG-NH_2 nanoparticles at excitation 350 nm.

3.2 Drug Loading and Release

DOX·HCl, an anticancer drug, was used to load into FMSN-PEG-NH_2 nanoparticles. The loading efficiency of DOX on FMSN -PEG-NH_2 nanoparticles was 60.8 % and the drug-loading content was 90 μg/mg. The in vitro drug release profile of DOX from DOX-FMSN-PEG-FA nanoparticles in different PBS (pH= 5.0, 7.4) at 37 °C were shown in Figure 6. After 72 h, about 65.5% of the DOX is released in the pH 5.0, while 14.8% of the DOX is released in the pH 7.4. This difference in release rates should mainly be attributed to the different solubility of DOX in the different pH buffer solution. It is known that DOX is dissolved in water at low pH, but insoluble in alkaline environment. As a result, the insoluble DOX could not be freely distributed out of mesopores at pH=7.4 [44].

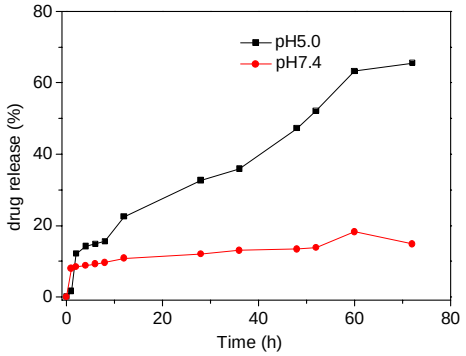

Figure 6. Cumulative drug release from DOX-FMSN-PEG-FA nanoparticles in PBS of different pH values.

3.3 In Vitro Cytotoxicity of the nanoparticles

To evaluate the biocompatibility of the FMSN-PEG-NH_2 nanoparticles, the particle-induced cytotoxic effects on Hep2 cells were measured by MTT assay. As shown in Figure 7A, the cell viability were all greater than 90% after a 24 h exposure. These datas show that the FMSN-PEG-NH_2 nanoparticles have a small level of cytotoxicity under the measured concentration range up to 100 μg/ml as a drug delivery vehicle.

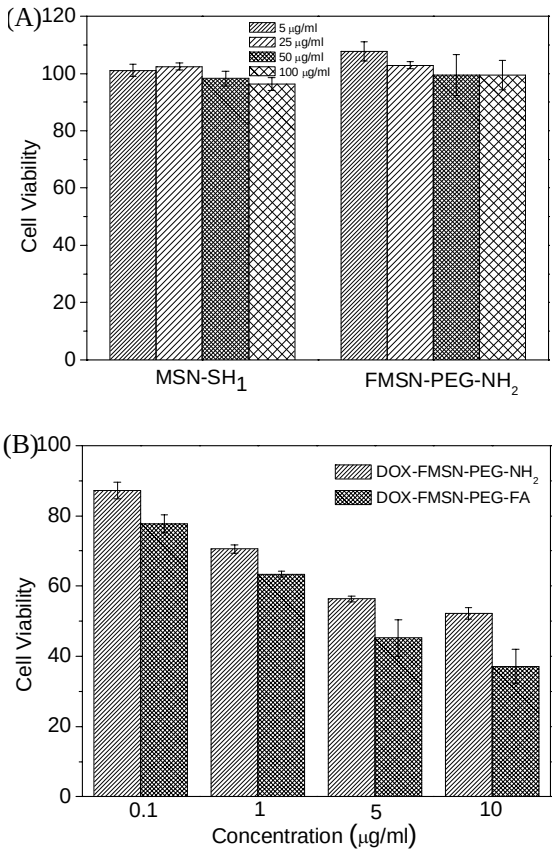

Figure 7. (A) Cell viabilities of the MSN-SH_1 and FMSN-PEG-NH_2 against Hep2 cells. (B) Cell viabilities of DOX-FMSN-PEG-NH_2 and DOX-FMSN-PEG-FA nanoparticles against Hep2 cells at different concentrations for 24 h.

Table 2. Half-maximal inhibitory concentrations (IC50) of DOX-FMSN-PEG-NH_2, DOX-FMSN-PEG-FA nanoparticles after 24 h incubation with cells.

Cell line	DOX-FMSN-PEG-NH_2 (μg/mL)	DOX-FMSN-PEG-FA (μg/mL)
Hep2 cells	10.708	3.028

In order to confirm the folate-receptor-mediated targeted drug delivery, the cytotoxic effect of DOX-FMSN-PEG-NH_2 and DOX-FMSN-PEG-FA nanoparticles at different concentrations against Hep2 cells are tested, and then determined the half maximal inhibitory concentration (IC50) of DOX (Table 2). Figure 7B shows that both DOX-FMSN-PEG-NH_2 and DOX-FMSN-PEG-FA nanoparticles could inhibit the growth of cells after incubation 24 h, which presented dose-dependent cytotoxicity behavior. But the DOX-FMSN-PEG-FA nanoparticles exhibit higher cytotoxicity than the DOX-FMSN-PEG-NH_2 nanoparticles. The measurement of IC50 dose of DOX-FMSN-PEG-NH_2 resulted in the relatively high value (IC50 = 10.708 μg/mL). Targeting DOX-FMSN-PEG-FA conjugates specifically to Hep2 cells led to the statistically significant increase in toxicity and decrease in IC50 value (IC50 = 3.028 μg/mL). These datas correlate well with the results of figure 7B.

Because DOX-FMSN-PEG-FA nanoparticles can be taken up by receptor-mediated endocytosis, Hep2 cells can take up more DOX-FMSN-PEG-FA nanoparticles than DOX-FMSN-PEG-NH_2 nanoparticles, which induces more cell death. Meanwhile, the results of the CLSM images also prove receptor-mediated endocytosis of the nanoparticles. Figure 8 shows the cell uptake of DOX-FMSN-PEG-NH_2 and DOX-FMSN-PEG-FA nanoparticles in Hep2 cells after incubation of 12 h under the same condition. The red-emitting points distributed in cells from DOX-FMSN-PEG-FA nanoparticles are much more than DOX-FMSN-PEG-NH_2 nanoparticles. In addition, owing to the release of DOX from DOX-FMSN-PEG-FA is more than DOX-FMSN-PEG-NH_2, the fluorescence intensity in the nucleus is higher than DOX-FMSN-PEG-NH_2 nanoparticles.

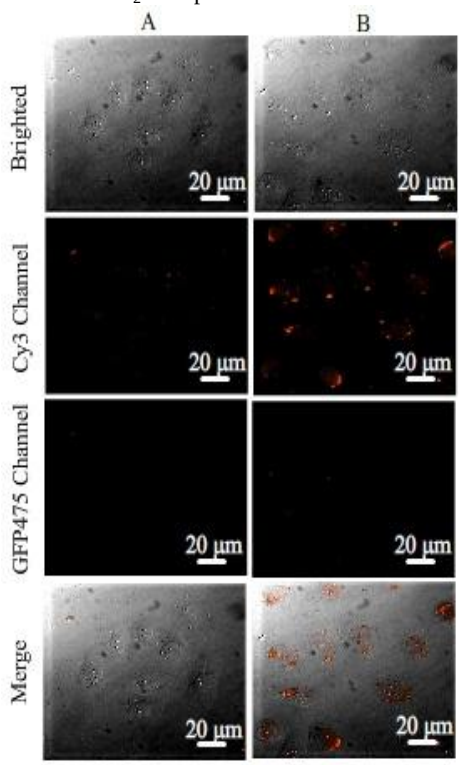

Figure 8. Confocal luminescence images of Hep2 cells were incubated with DOX-FMSN-PEG-NH_2 (A) and DOX-FMSN-PEG-FA (B) nanoparticles at 37 °C for 12 h (DOX concentration = 2 μg/mL).

3.4 FRET between FMSN nanoparticles and DOX

Figure 9A shows the emission spectrum of FMSN and the absorption spectrum of DOX. Obviously, the spectral overlap between emission of donor FMSN nanoparticles at 500 nm and the broad absorbance of acceptor DOX around 484 nm enable

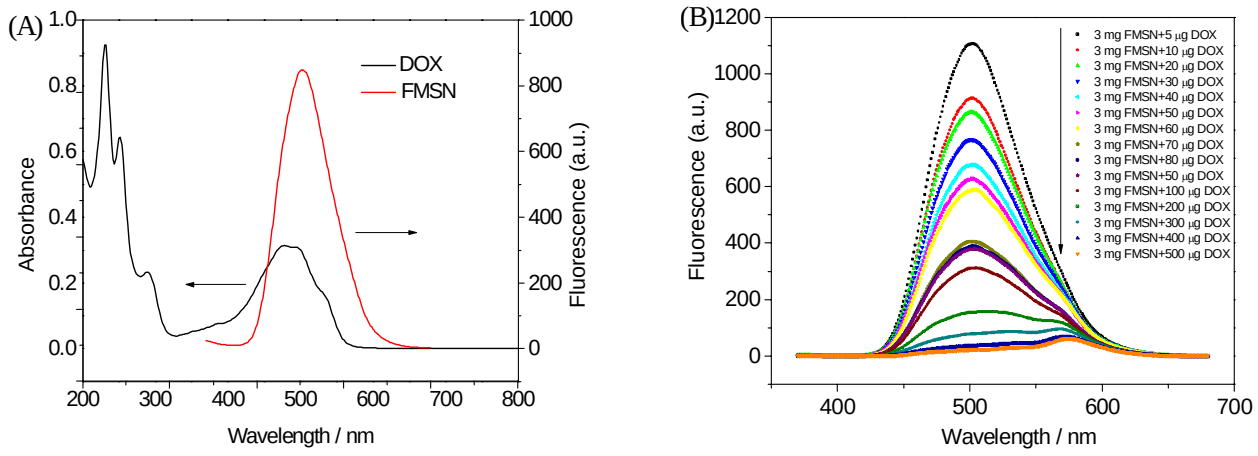

Figure 9. (A)The emission spectrum of FMSN and the UV-vis absorption spectrum of DOX. (B) The emission spectra of FMSN (3 mg) after reaction with DOX at different quantity.

energy transfer to occur between the FRET pair. As shown in Figure 9B, sequential decreases the fluorescence intensity of FMSN at 500 nm were observed when a fixed quanlity of FMSN (3 mg) was incubated with an increasing the quantity of DOX from 0 to 500 μg. Quenching the fluorescence of FMSN by DOX attributed to the energy transfer from FMSN to DOX. Thus the existence of FRET between FMSN nanoparticles and DOX is confirmed.

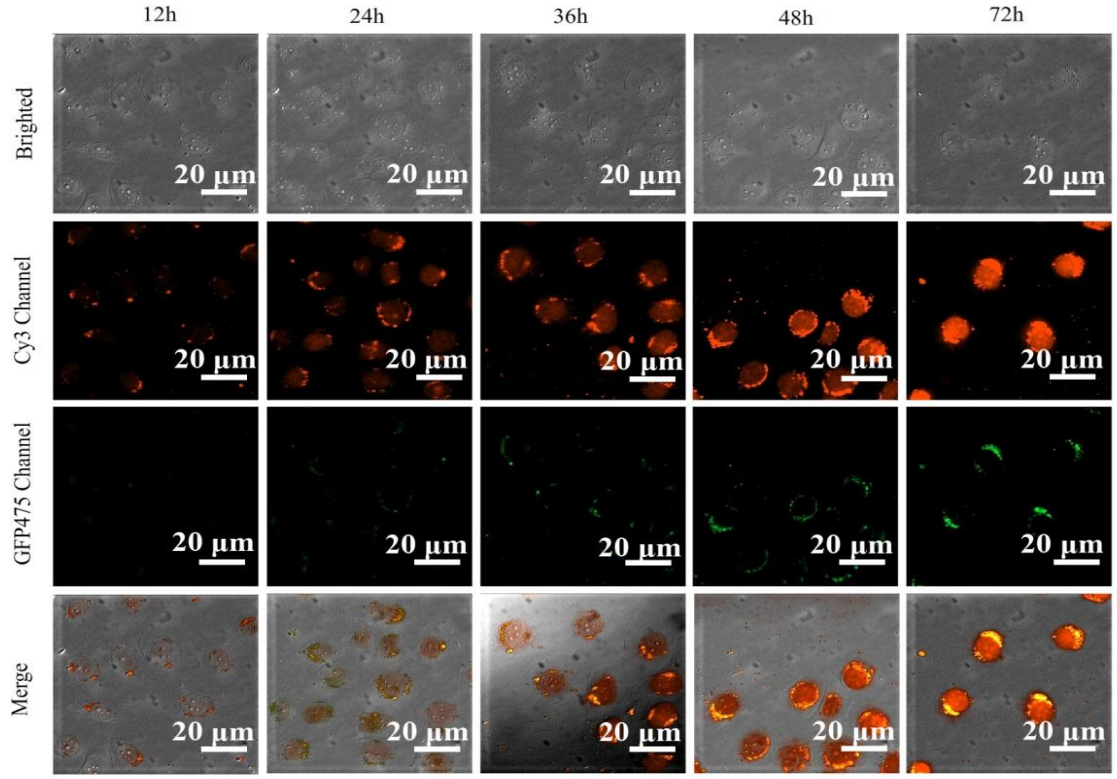

Figure 10. Confocal images of Hep2 cells incubated with DOX-FMSN-PEG-FA nanoparticles for 12 h, 24 h, 36 h, 48 h, 72 h at 37 °C (DOX concentration = 2 μg/mL).

3.5 Intracellular monitoring/imaging drug release using FRET

The intracellular drug release process was evaluated after incubation DOX-FMSN-PEG-FA with Hep2 cells by CLSM in optical windows between Cy3 channel and GFP475 channel. In the first 12 h, only a few nanoparticles could be uptaken by Hep2 cells and accumulated near the cell nucleus. The red fluorescence of DOX-FMSN-PEG-FA nanoparticles was observed in both the cytoplasm and the cell nucleus in the Cy3 channel, while almost no green fluorescence was observed in the GFP475 channel in the perinuclear region, signifying FRET is on with high efficiency (the first column in Figure 10). After 12 h, a relative strong intensity of DOX fluorescence was seen in the cell nucleus while a weak green fluorescence was observed in the cytoplasm suggesting the efficiency of FRET between DOX and DOX-FMSN-PEG-FA nanoparticles decreased relatively due to the release of DOX from DOX-FMSN-PEG-FA nanoparticles (the second column in Figure 10). With time processing (36-72 h), more and more nanoparticles were taken up by receptor-mediated endocytosis and appeared in the perinuclear region. Owing to the gradual release of DOX from DOX-FMSN-PEG-FA nanoparticles, the intensity of green fluorescence of FMSN in the GFP475 channel gradually recovered. Meanwhile, the red fluorescence in the cell nucleus also became stronger (the third to fifth column in Figure 10).

The above results prove that the nanoparticles could be uptake effectively by Hep2 cells through receptor-mediated endocytosis. The release of DOX from DOX-FMSN-PEG-FA nanoparticles pass through the nuclear membrane into nucleus and eventually accumulate in the cell nuclei to kill the cell by inhibiting macromolecular biosynthesis.

Conclusions

In summary, we have designed a multifunctional drug delivery system based on DOX-FMSN-PEG-FA nanoparticles combining receptor-mediated targeting, therapy and real-time monitoring/imaging of intracellular drug release through FRET mechanism. In vitro cell cytotoxicity results suggest that DOX-FMSN-PEG-FA nanoparticles exhibit greater cytotoxicity than DOX-FMSN-PEG-NH_2 nanoparticles due to the increase of cell uptake by receptor-mediated endocytosis. The quenching and recovery of the drug carrier could serve as an optical probe to monitor intracellular release of doxorubicin. Such drug delivery

system has potential applications in targeted anticancer drug delivery, imaging for cancer therapy.

Acknowledgements

We gratefully acknowledge financial supports from the National Natural Science Foundation of China (Grant number: 21035005).

Notes and references

Key Laboratory of Luminescent and Real-Time Analytical Chemistry (Southwest University), Ministry of Education, College of Pharmaceutical Sciences, Southwest University, Chongqing, 400715, P. R. China., Tel: +86 23 6825 4659; Fax: +86 23 68367257; E-mail: chengzhi@swu.edu.cn

† Electronic Supplementary Information (ESI) available: [details of any supplementary information available should be included here. See DOI: 10.1039/b000000x/

‡ Footnotes should appear here. These might include comments relevant to but not central to the matter under discussion, limited experimental and spectral data, and crystallographic data.

1 Cheng Z., A. Al Zaki, J. Z. Hui, V. R. Muzykantov, A. Tsourkas. *Science*. 2012, **338**, 903-910.

2 Horcajada P., T. Chalati, C. Serre, B. Gillet, C. Sebrie, T. Baati, et al. *Nat. Mater*. 2010, **9**, 172-178.

3 Vivero-Escoto J. L., I. I. Slowing, B. G. Trewyn, V. S. Y. Lin. *Small*. 2010, **6**, 1952-1967.

4 Gada K., V. Patil, R. Panwar, A. Hatefi, B.-A. Khaw. *Drug Deliv. Transl. Res*. 2012, **2**, 65-76.

5 Du J.-Z., X.-J. Du, C.-Q. Mao, J. Wang. *J. Am. Chem. Soc*. 2011, **133**, 17560-17563.

6 Malam Y., M. Loizidou, A. M. Seifalian. *Trends Pharmacol. Sci*. 2009, **30**, 592-599.

7 Pradhan P., J. Giri, F. Rieken, C. Koch, O. Mykhaylyk, M. Döblinger, et al. *J. Control. Release*. 2010, **142**, 108-121.

8 Ganta S., D. Deshpande, A. Korde, M. Amiji. *Mol. Memb. Biol*. 2010, **27**, 260-273.

9 Sun H. W., K. Y. Liu, W. Liu, W. X. Wang, C. L. Guo, B. Tang, et al. *Int. J. Nanomed*. 2012, **7**, 5529-5543.

10 Kurtoglu Y. E., R. S. Navath, B. Wang, S. Kannan, R. Romero, R. M. Kannan. *Biomaterials*. 2009, **30**, 2112-2121.

11 Yuan H., K. Luo, Y. Lai, Y. Pu, B. He, G. Wang, et al. *Mol. Pharmaceut*. 2010, **7**, 953-962.

12 Wu W., T. Zhou, A. Berliner, P. Banerjee, S. Zhou. *Chem. Mater*. 2010, **22**, 1966-1976.

13 Gupta H., T. Velpandian, S. Jain. *J. Drug Target*. 2010, **18**, 499-505.

14 Alexander C. M., M. M. Maye, J. C. Dabrowiak. *Chem. Commun*. 2011, **47**, 3418-3420.

15 Kim M., K.-S. Ock, K. C. Cho, S.-W. Joo, S. Y. Lee. *Chem. Commun*. 2012.

16 Adeli M., R. S. Sarabi, R. Yadollahi Farsi, M. Mahmoudi, M. Kalantari. *J. Mater. Chem*. 2011.

17 Gu Y.-J., J. Cheng, C. W.-Y. Man, W.-T. Wong, S. H. Cheng. *Nanomedicine*. 2012, **8**, 204-211.

18 Savla R., O. Taratula, O. Garbuzenko, T. Minko. *J. Control. Release*. 2011, **153**, 16-22.

19 Chakravarthy K. V., B. A. Davidson, J. D. Helinski, H. Ding, W.-C. Law, K.-T. Yong, et al. *Nanomedicine*. 2011, **7**, 88-96.

20 Suriamoorthy P., X. Zhang, G. Hao, A. Joly, S. Singh, M. Hossu, et al. *Cancer Nano*. 2010, **1**, 19-28.

21 Trewyn B. G., I. I. Slowing, S. Giri, H.-T. Chen, V. S. Y. Lin. *Acc. Chem. Res*. 2007, **40**, 846-853.

22 Descalzo A. B., R. Martínez-Máñez, F. Sancenón, K. Hoffmann, K. Rurack. *Angew. Chem. Int. Ed*. 2006, **45**, 5924-5948.

23 Chen Y., H. Chen, S. Zhang, F. Chen, L. Zhang, J. Zhang, et al. *Adv. Funct. Mater*. 2011, **21**, 270-278.

24 Zhang Q., F. Liu, K. T. Nguyen, X. Ma, X. Wang, B. Xing, et al. *Adv. Funct. Mater*. 2012, **22**, 5144-5156.

25 Meng H., M. Xue, T. Xia, Y.-L. Zhao, F. Tamanoi, J. F. Stoddart, et al. *J. Am. Chem. Soc*. 2010, **132**, 12690-12697.

26 Wang T.-T., F. Chai, C.-G. Wang, L. Li, H.-Y. Liu, L.-Y. Zhang, et al. *J. Colloid. Interface Sci*. 2011, **358**, 109-115.

27 Sun L., Y. Zang, M. Sun, H. Wang, X. Zhu, S. Xu, et al. *J. Colloid. Interface Sci*. 2010, **350**, 90-98.

28 Gruenhagen J. A., C.-Y. Lai, D. R. Radu, V. S. Y. Lin, E. S. Yeung. *Appl. Spectrosc*. 2005, **59**, 424-431.

29 Jares-Erijman E. A., T. M. Jovin. *Nat. Biotech*. 2003, **21**, 1387-1395.

30 Szöllosi J., S. Damjanovich, L. Mátyus. *Cytometry*. 1998, **34**, 159-179.

31 Didenko V. V. *Biotechniques*. 2001, **31**, 1106-1121.

32 Bednarkiewicz A., M. Nyk, M. Samoc, W. Strek. *J. Phys. Chem. C*. 2010, **114**, 17535-17541.

33 Guo H., N. M. Idris, Y. Zhang. *Langmuir*. 2011, **27**, 2854-2860.

34 Huang X., S. Lee, X. Chen. *Am. J. Nucl. Med. Mol. Imaging*. 2011, **1**, 3-17.

35 Dennis A. M., W. J. Rhee, D. Sotto, S. N. Dublin, G. Bao. *ACS Nano*. 2012, **6**, 2917-2924.

36 Xue M., X. Wang, L. Duan, W. Gao, L. Ji, B. Tang. *Biosens. Bioelectron*. 2012, **36**, 168-173.

37 Lai J., B. P. Shah, E. Garfunkel, K.-B. Lee. *ACS Nano*. 2013, **7**, 2741-2750.

38 Kobler J., K. Möller, T. Bein. *ACS Nano*. 2008, **2**, 791-799.

39 Möller K., J. Kobler, T. Bein. *Adv. Funct. Mater*. 2007, **17**, 605-612.

40 Li H., Y. Fu, L. Zhang, X. Liu, Y. Qu, S. Xu, et al. *Micropor. Mesopor. Mater*. 2012, **151**, 293-302.

41 Luo Z., K. Cai, Y. Hu, L. Zhao, P. Liu, L. Duan, et al. *Angew. Chem. Int. Ed*. 2011, **50**, 640-643.

42 Gavrilko T., R. Fedorovich, G. Dovbeshko, A. Marchenko, A. Naumovets, V. Nechytaylo, et al. *J. Mol. Struct*. 2004, **704**, 163-168.

43 Wu H., S. Zhang, J. Zhang, G. Liu, J. Shi, L. Zhang, et al. *Adv. Funct. Mater*. 2011, **21**,1850-1862.

44 Chang B., J. Guo, C. Liu, J. Qian, W. Yang. *J. Mater. Chem*. 2010, **20**, 9941-9947.

A graphic abstract

for

Real-time Imaging of Intracellular Drug Release from Mesoporous Silica Nanoparticles Based on Fluorescence Resonance Energy Transfer

Jun Wang, Peng Pei Gao, Xiao Xi Yang, Ting Ting Wang, Jian Wang* and Cheng Zhi Huang*

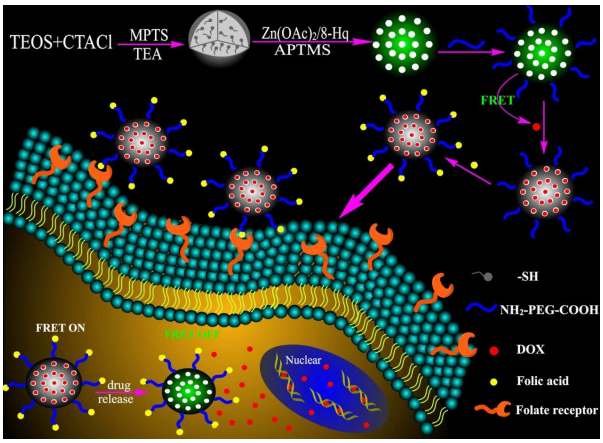

A targeted cancer therapy, imaging and sensing system is designed based on doxorubicin (DOX)-loaded green fluorescence mesoporous silica nanoparticles (FMSN) conjugated with folic acid (FA) by linking α-amine-ω-propionic acid hexaethylene glycol, achieving the real-time monitoring of intracellular drug release based on fluorescence resonance energy transfer.